A broadband single-chip transceiver for multi-nuclear NMR probes

3 authors:

Marco Grisi
École Polytechnique Fédérale de Lausanne
12 PUBLICATIONS   **111** CITATIONS

SEE PROFILE

Gabriele Gualco
École Polytechnique Fédérale de Lausanne
6 PUBLICATIONS   **33** CITATIONS

SEE PROFILE

Giovanni Boero
École Polytechnique Fédérale de Lausanne
101 PUBLICATIONS   **1,679** CITATIONS

SEE PROFILE

Some of the authors of this publication are also working on these related projects:

Focused electron Beam Induced Processing FEBIP View project

innovative devices for electron spin resonance on small samples View project

A broadband single-chip transceiver for multi-nuclear NMR probes

Marco Grisi,[a)] Gabriele Gualco, and Giovanni Boero
Ecole Polytechnique Fédérale de Lausanne (EPFL), Lausanne CH-1015, Switzerland

In this article, we present an integrated broadband complementary metal-oxide semiconductor single-chip transceiver suitable for the realization of multi-nuclear pulsed nuclear magnetic resonance (NMR) probes. The realized single-chip transceiver can be interfaced with on-chip integrated microcoils or external LC resonators operating in the range from 1 MHz to 1 GHz. The dimension of the chip is about 1 mm^2. It consists of a radio-frequency (RF) power amplifier, a low-noise RF preamplifier, a frequency mixer, an audio-frequency amplifier, and fully integrated transmit-receive switches. As specific example, we show its use for multi-nuclear NMR spectroscopy. With an integrated coil of about 150 μm external diameter, a ^{1}H spin sensitivity of about 1.5×10^{13} spins/Hz$^{1/2}$ is achieved at 7 T. © *2015 AIP Publishing LLC.* [http://dx.doi.org/10.1063/1.4916206]

I. INTRODUCTION

Nuclear magnetic resonance (NMR) techniques are widely employed in chemistry, physics, biology, medicine, and material science for a large variety of studies.[1–3] Although diffused and very powerful, costs and dimensions of the necessary instrumentation limit its use, making of it a last resort for those cases where cheaper techniques are not available. In principle, the use of low-cost NMR spectrometers and imagers can reach a huge number of applications: from real-time diagnostics (e.g., on skin, biological samples, or tendons)[4–6] to quality control of various products (e.g., elastomers or olive oils).[7,8] In the last few years, low-cost NMR systems were proposed on the market in the attempt of fulfilling these needs.[9,10]

Given a static external magnetic field B$_0$, the NMR frequency is $\nu_0 = (\gamma/2\pi)B_0$, where γ is the gyromagnetic ratio of the target nucleus (($\gamma/2\pi) \approx 42.6$ MHz/T for protons).[11] In order to obtain a high signal-to-noise ratio (SNR) and access the information hidden in NMR spectra, strong and homogeneous magnetic fields are required.[12,13] The realization of strong and homogeneous miniaturized magnets is the main obstacle towards low-cost portable NMR tools, possibly solved by Halbach configurations of permanent magnets.[14,15] NMR systems also require relatively complex RF electronics for resonance excitation and signal detection. The design of electronic micro-chips for NMR purposes has the aim to shrink the size of electronics for low-cost NMR spectrometers[16–19] and to combine microcoils with integrated receivers in order to achieve probes parallelization and high spin sensitivity.[20–23]

The first integrated probe was proposed for magnetometry purposes and employed integrated pick-up-coils coupled to receivers, with the excitation operated by a second inductively decoupled coil.[24] Receiver-only chips, with the whole electronics buried below integrated microcoils, were proposed

as optimal choice for micro-imaging,[23] parallel imaging arrays,[20] and probes for surgical guidance.[22] The realization of integrated transceivers for NMR purposes, of which there are only a few examples,[16–18] also included integrated pulse sequencers aiming at miniaturizing the size and abating the costs of the overall electronics needed to build spectrometers.

This report describes a broadband single-chip transceiver, whose combination with multi-frequency probes provides a simple, but effective and versatile, low-cost electronic interface for NMR probes. We show its employment in combination with both external and integrated microcoils. As specific examples, we performed multi-nuclear NMR spectroscopy on solids and liquids.

Our single-chip transceiver consists of a RF power amplifier, a RF low-noise preamplifier, a frequency mixer, an audio-frequency (AF) amplifier, and fully integrated transmit-receive switches. One issue of integrated transceivers is to connect efficiently transmission (TX) and reception (RX) electronics with the excitation-detection coil. In previous works, switches were placed in series with the transmitter, implying power losses in TX mode.[16,18] The topology used to realize our switches allows, as well as that in Ref. 17, power transmission without power loss. More than 50 dB isolation is provided between TX and RX, and both channels operate with best performance from 1 MHz to 1 GHz.

We realized probes for samples of volumes of the order of 100 nl (using an external coil) and 500 pl (using an integrated microcoil). Recently, non-resonant microcoils were indicated as an option to realize volume-limited (25 nl) multi-nuclear NMR probes.[25] Nevertheless, at the same scale, it is still possible to use resonant micro-solenoids capable of high spectral resolution and spin sensitivity.[26] Indeed, when possible, the use of LC resonators allows a lossless intrinsic gain between the coil and the receiver, definitively advantageous in terms of SNR.[12] An issue in multi-frequency resonant probes is to tune the same resonator at different frequencies. Our single-chip transceiver is interfaced with a resonant coil via a matching network where reversed biased

a)marco.grisi@epfl.ch

diodes are employed as voltage controlled capacitors, allowing a frequency range where the ratio between the maximum and minimum frequency is up to a factor of four. The fully integrated probe, on the other hand, is designed for volumes where it is hardly possible to realize multi-frequency LC resonators. Thus, a non-resonant microcoil is used. As future prospective, our work can serve as base to realize low-cost NMR interfaces and high sensitivity micro-probes arrays for micro-imaging and mass limited spectroscopy purposes.

Section II is dedicated to the description of the integrated electronics and probes design. In Sec. III, we introduce the basics of pulsed NMR and describe the experimental setup. In Sec. IV, we present multi-nuclear spectroscopy experimental results obtained with the realized probes.

II. ELECTRONICS DESIGN

In Fig. 1(a), we show photographs of the single-chip transceivers. The chips, realized with a 2P6M complementary metal-oxide semiconductor (CMOS) 130 nm process provided
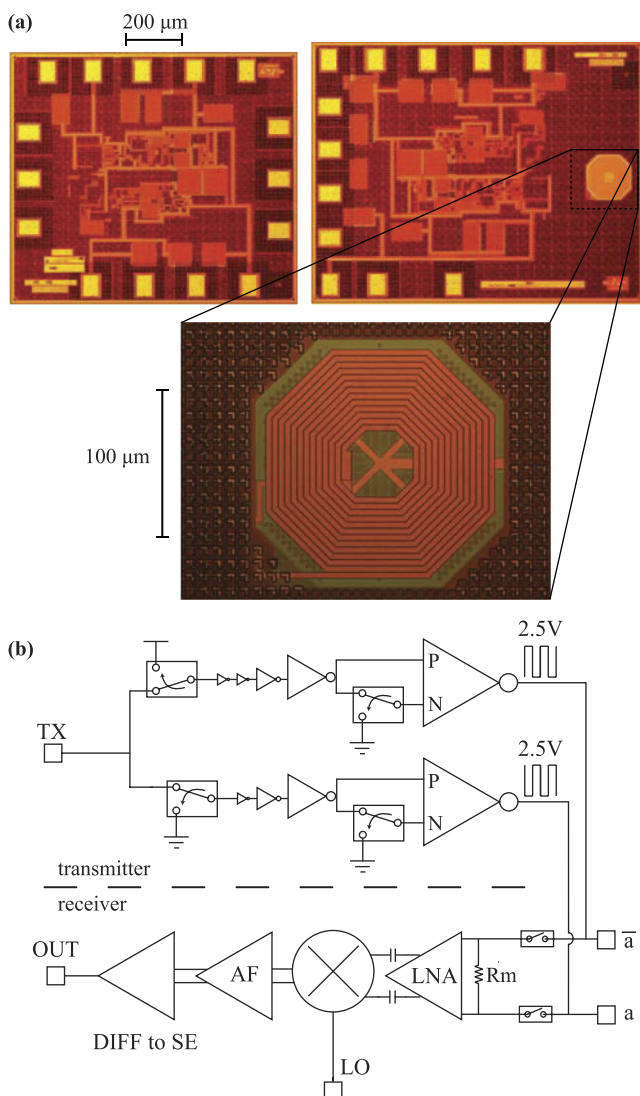

FIG. 1. (a) Photograph of the single-chip transceivers for both external (left) and integrated (right) coil. (b) Block diagram of the single-chip transceiver.

by STMicroelectronics, have dimensions of about 1 mm^2. Fig. 1(b) shows the block diagram of the single-chip transceiver where transmitter and receiver are connected to the integrated or external coil at two nodes a and ā.

A. Transmitter

The transmitter design, inspired by previous reports, consists of two differential chains of inverters.[16] Our integrated switches allow commutation between TX and RX in some ns and provide more than 50 dB isolation between the two channels. No switches are used in series with the output stage of the transmitter, which consequently operates with no power losses. Fig. 1(b) shows the case in which the TX mode is selected. In the RX mode, the two inverter chains are in stand-by, no current is drawn from their DC source, and the four last transistors of the transmitter act as open switches with impedances of about 200 kΩ. We used 2.5 V I/O transistors, which operate at the largest voltage of the technology employed. During transmission, the inverters impose differential squared waves in a and ā, both toggling between ground and 2.5 V. The output impedance of the transmitter is $Z_s = 50$ Ω. The power delivered to the probe depends on the impedance Z between nodes a and ā in TX mode, and it is $P = V_{rms}^2 / |Z_s + Z|$, where $V_{rms} \approx 1.8$ V for sinusoids of amplitude 2.5 V. When we use an external coil, we tune it at the working frequency and match its impedance to $R_m = 320$ Ω. In these conditions, the transmitted current is about 10 mA and the transmitted power is about 10 mW. When we use the integrated coil, the transmitted current is about 20 mA and the transmitted power is about 20 mW at 300 MHz (see description of the integrated coil below). The transmitter current limit is 70 mA.

B. Receiver

The receiver consists of a low-noise RF amplifier (LNA), a double balanced Gilbert mixer, a Miller AF amplifier, and a last amplification stage where the signal is converted from differential to single-ended. Integrated mixed signal circuits suffer of common mode noise due to digital switching noise on the supply line. For this reason, the whole receiver is designed as a fully differential system. The differential-to-single-ended conversion is done once the common mode noise is much smaller than the amplified differential one. The detailed schematics of LNA, mixer, and AF amplifier can be found in the supplementary material (SI.B).[27]

The LNA has a gain of 35 dB and it is AC coupled to the mixer in order to avoid offset problems. Mixer and AF part have gain of 19 dB. Hence, the overall gain of the receiver is 54 dB. The receiver consumes a current of 14 mA from a 1.5 V DC source.

The wideband fully differential LNA is the first element interfaced with the coil. Its bandwidth is 1–300 MHz and its frequency-dependent input impedance is $Z_{LNA} = 1/i\omega C_{gs}$, with $C_{gs} \approx 0.5$ pF. The large size of the input transistors, whose areas measure 150 (P-MOS) and 63 (N-MOS) μm^2, is necessary to reduce the $1/f$ noise component at low frequencies. When the coil is external, a resistor $R_m = 320$ Ω fixes the real part of the input impedance and protects the

LNA from the energy discharge associated with TX to RX switching. When the coil is integrated, there is no resonator and no impedance matching, and R_m is increased to 20 kΩ to improve noise performance (see Sec. IV A). The impedance of the two switches connected to a and $\bar{a}$ is about 10 Ω in RX mode and 6 kΩ in TX mode. Hence, the contribution of the switches to the electronic noise in RX mode is negligible.

C. Dead-time

During transmission, the resonating RLC network stores a certain amount of energy, whose ratio with the energy dissipated per unit cycle defines the quality factor $Q = \omega L/R_C$, where ω is the resonating angular frequency, L is the inductance of the coil, R_C is its resistance.[28] Switching from TX to RX, the stored energy dissipates and causes the saturation of the receiver for a time which depends on both the time needed by the resonator to discharge and the time needed by the receiver to recover from its saturation condition. The combination of these two delays gives rise to the so called dead-time, defined as the time interval between the end of the excitation and the beginning of useful signal acquisition. In an optimal design, the recovery of the receiver should be negligible and the dead-time should be mainly determined by the discharge time of the resonator and the gain of the electronics. The decay time of the discharging resonator is $T_d = L/R_C = Q/\omega_0$. The recovery time of the receiver is of the order of the inverse of its AF bandwidth, which in our case is about 4 MHz. The measured recovery time of our receiver is about 1 μs. After excitation, the NMR signal decays exponentially with the relaxation time T_2. Relaxation times in liquids can be as large as 10 s, while solids and elastomers have relaxation times between tens of μs and some ms. It is thus clear that having a short dead-time is necessary to allow pulsed experiments on a broad variety of samples.

D. External coil

Fig. 2(a) shows a schematic of a multi-frequency probe, where matching and tuning capacitors C_m and C_t are adjusted by two voltage sources V_m and V_t on reverse-biased varicap diodes $D1$ and $D2$. The external probe is fully differential to reject the common mode noise. Fig. 2(b) shows the equivalent circuit where, essentially, a coil is interfaced with a real impedance R_m. Varying C_m and C_t, the impedance across nodes a and $\bar{a}$ can be transformed until it matches R_m.[28] In our probe, C_m and C_t have a dynamic range (defined as C_{max}/C_{min}) of about 16. The main drawback in using diodes as capacitors is that, during transmission, large signals are applied across the coil inducing for limited time forward bias of the diodes, hence dissipating some transmitted power. This particular issue can have severe consequences on the performance of the probe and it is more relevant when using coils with high Q factor: a larger Q factor implies larger voltage signals across the coil and thus more undesired power dissipation (see discussion in Sec. IV B).

The choice of the matched impedance is important when a fixed and relatively small power is available in transmission. Indeed, it is possible to show that (see supplementary material
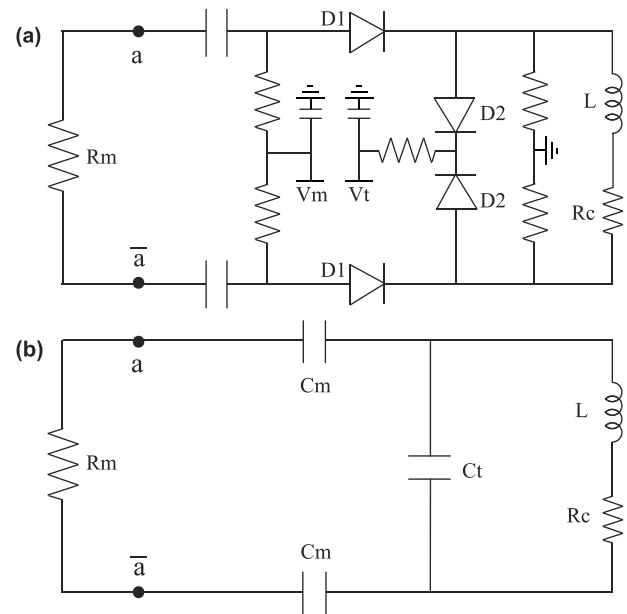

FIG. 2. (a) Multi-frequency probe: the tuning and matching capacitances are given by reverse-biased varicap diodes and are regulated by the control voltages V_m and V_t. V_m is negative and V_t is positive, their absolute value ranging between 0 and 25 V. $D1$ (matching): NXP BB181 and $D2$ (tuning): NXP BB182. (b) Equivalent circuit.

SI.A)[27] the process of impedance transformation includes an intrinsic gain $G_{int} = \sqrt{R_m/4R_C}$ from the coil to the nodes a and $\bar{a}$, indicating as optimal choice a high matched impedance to reduce the contribution of the noise of the electronics. It is also shown that the pulse length necessary to reach the maximum signal condition is $\tau_{\pi/2} = \pi\sqrt{R_mR_C}/\sqrt{2}\gamma B_u V_{rms}$ indicating a small matched impedance as preferable choice. Thus, a higher matched impedance is convenient when receiving but inconvenient when transmitting with a fixed limited power. In our design, the choice $R_m = 320$ Ω was judged to be a good compromise between pulse lengths and noise performance.

E. Integrated coil

The integrated coil shown in Fig. 1(a) is realized using the top four copper metals of the integrated circuit technology. The number of turns (22 in total), their diameter, and their width are optimized for cubic samples with edges of 50 μm. The Si_3N_4/SiO_2 passivation, separating sample and coil, is 1.1 μm thick. The 13 turns in the highest metal are 0.9 μm thick and 3.6 μm wide. The remaining three metals have three turns each, 0.35 μm thick, and 6.4 μm wide. The DC inductance is 54 nH and the DC resistance is 60 Ω. Since the skin depth in copper at 300 MHz is significantly larger than the metal thickness, the resistance at 300 MHz is marginally higher than the DC value.

III. EXPERIMENTAL SETUP

When placed into an external static magnetic field B_0 along a direction $\hat{z}$, spins of paramagnetic nuclei precess about the static field at the Larmor angular frequency $\omega_0 = \gamma B_0$

and their energy minimum favors their partial alignment along $\hat{z}$, giving a macroscopic magnetization $M_0 = N_s(I+1)I\gamma^2\hbar^2B_0/(3k_BT)$, N_s being the density of spins, I being the nuclear spin, T being the temperature of the sample.[2] It is possible to exploit a resonant phenomenon by applying a field B_1 oscillating at the Larmor frequency along a direction perpendicular to $\hat{z}$. In doing so, the orientation in space of the sample magnetization M changes, rotating in space with an angular velocity $\omega_1 = \gamma B_1$. After an excitation time τ, the angle ϑ between M and $\hat{z}$ will be $\vartheta = \gamma B_1\tau$.[2] When B_1 is suddenly shut down, the magnetization relaxes towards its thermal equilibrium condition keeping its precession at frequency ω_0 about $\hat{z}$. An electromotive force, which survives until the spins precession remains coherent, is induced by Faraday's law in any inductor placed in proximity. A basic NMR experiment uses a single coil to excite the resonance and pick-up the free induction decay (FID) signal, whose initial amplitude is given by $s_0 = \omega_0 M_0 V_s B_u \sin\vartheta$,[12] where B_u is the field per unit current (unitary field) of the coil and V_s the sample volume. The maximum signal is obtained when the magnetization of the sample is rotated by $\vartheta = \pi/2$ and the excitation field B_1 must be as high as possible in order to reach this condition in a short time compared to the nuclear relaxation times.[2] Having small excitation pulse lengths (a few μs) also guarantees uniform excitations of broad spectra. Fig. 3(a) illustrates a simple pulsed NMR experiment,
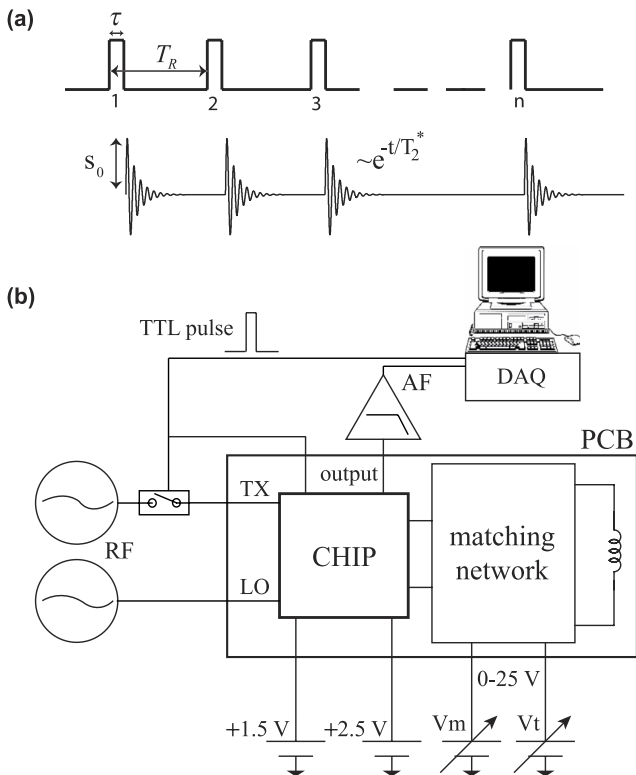
where n excitation pulses of length τ and n acquisitions are consecutively performed with a repetition time T_R. After each pulse, a signal with initial amplitude s_0 and typical decay time T_2^* is acquired. For a maximal signal in each measurement, the repetition rate T_R must be significantly larger than T_1, which is the time required to restore the thermal magnetization M_0. Usually called longitudinal (or spin-lattice) relaxation time, T_1 depends on both the sample and the external field. From the received signal, one can extract the amplitude s_0 proportional to the number of participating spins, the Larmor frequency dependent on the chemical structure,[29] and the effective relaxation time T_2^*. In liquids, the effective relaxation time is mainly due to the field inhomogeneity within the sample, which facilitates the loss of coherence between spins and thus the decay of the signal. With more complicated pulse sequences (e.g., the spin echo technique),[30] one can have access to the true relaxation time T_2, which reveals information concerning spin-spin interaction within the sample, ultimate cause of spin decoherence.[31]

Fig. 3(b) shows the block diagram of the setup used for our measurements. The single-chip transceiver is wire bonded to a printed circuit board (PCB). The transceiver is interfaced with the external excitation-detection coil via a matching network (see Fig. 2), while no other component is needed when the coil is integrated on-chip. For excitation and down-conversion, we can choose to use a single RF generator or two separate ones. The advantage of working with two RF generators is the on-resonance transmission, allowing both the use of long pulse lengths and a down-converted frequency far from the $1/f$ noise region. When using two separate RF sources, a pre-switch of the excitation signal is preferable to eliminate the weak parasitic signal due to TX to RX leakage. The output signal is amplified before acquisition. The gain and antialiasing low-pass filter of the external AF amplifier increase the effective dead-time of the system (up to 9 μs with a gain of 10^3 and low-pass filter at 300 kHz). Four DC
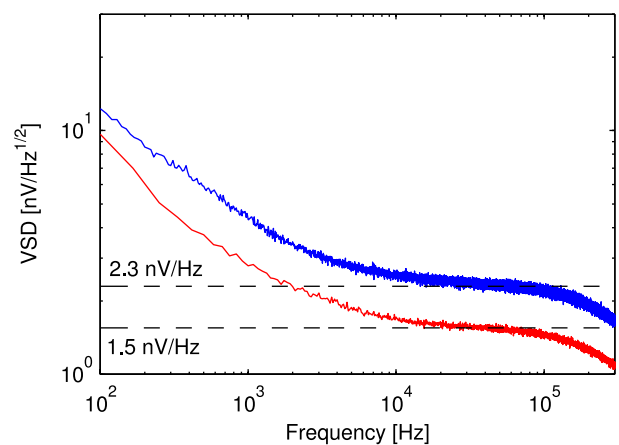

(a)

FIG. 3. (a) A schematics of a pulsed NMR experiment, where n pulsed experiments are performed with pulse length τ and repetition time T_R. The signal has an amplitude s_0 and an effective relaxation time T_2^*. (b) Block diagram of the complete NMR system. RF source: Anritzu MG3633A. AF amplifier: Stanford SR560. The printed circuit board (PCB) containing the single-chip transceiver is inserted into the 54 mm room-temperature bore of a Bruker 7.05 T superconducting magnet.

FIG. 4. Measured equivalent input noise voltage spectral density (*VSD*). Blue: noise with a 320 Ω resistor at receiver input. Red: noise with the integrated micro-coil at receiver input. The local oscillator (LO) frequency is 100 MHz at 0 dBm power. The acquisition is performed with sampling rate of 1.3 MHz and a 300 kHz antialiasing filter. The corner frequency is slightly dependent on the local oscillator frequency, with a value of 15 kHz at 300 MHz. The noise level measured at 50 kHz is independent from the local oscillator frequency in the range from 1 MHz to 1 GHz.
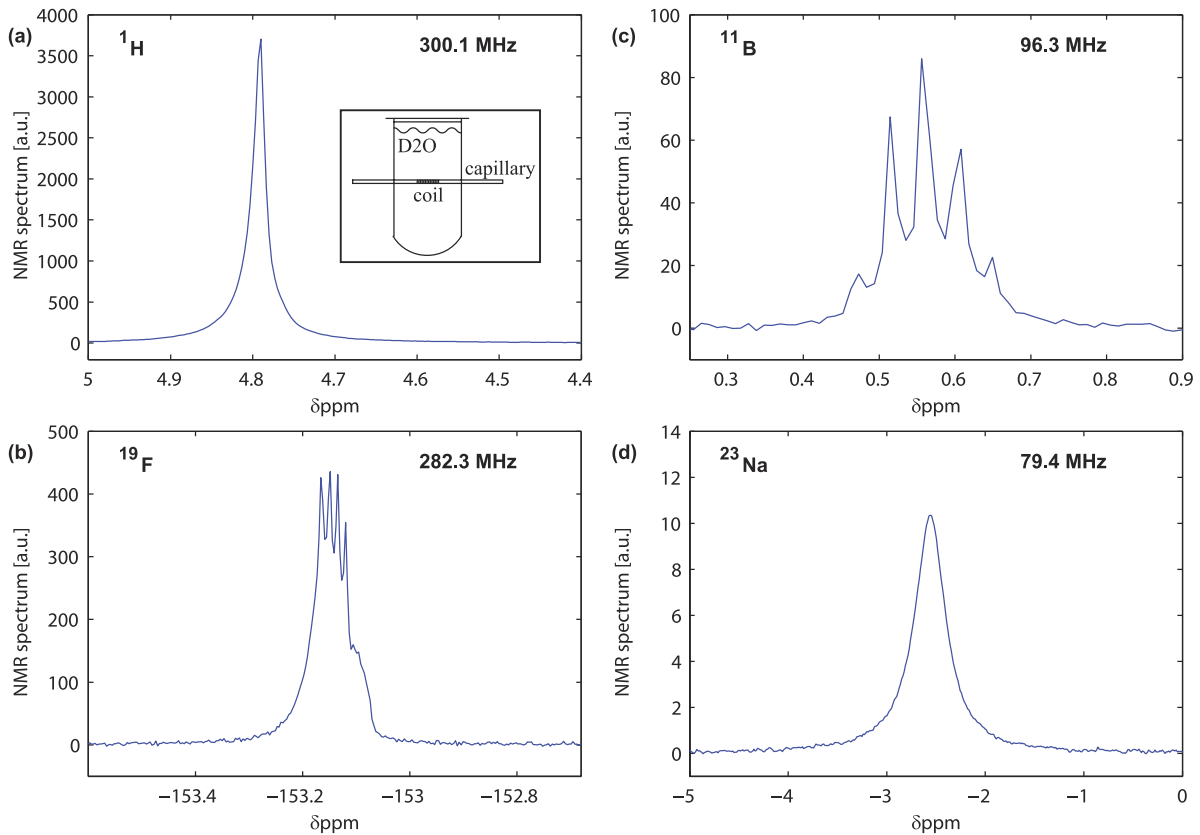
FIG. 5. Measurements with the external coil probe in a field $B_0 = 7.05$ T. Spectra are FFT real parts. For all measurements, we used a single coil matched and tuned at various frequencies using varicap diodes. The coil consists of 14 turns, 100 μm diameter enameled copper wire solenoid wrapped around a fused silica capillary (from Polymicro Technologies) having external diameter of 450 μm and internal diameter of 320 μm. The sample volume is 100 nl and contains NaBF$_4$ dissolved in H$_2$O with a concentration of 7.5 M. The coil is inserted in a 2 ml Eppendorf tube filled with D$_2$O for susceptibility matching. The acquisition is performed with sampling rate of 500 kHz. The AF external gain is 10^2 and the antialiasing filter frequency is 100 kHz. Each signal is down-converted at about 50 kHz. 7 μs of data are rejected. (a) ^{1}H spectrum, single measurement with $\tau = 12$ μs. (b) ^{19}F spectrum, single measurement with $\tau = 14$ μs. (c) ^{11}B spectrum, average of 20 measurements with $T_R = 15$ s and $\tau = 32$ μs. (d) ^{23}Na spectrum, average of 500 measurements with $T_R = 1$ s and $\tau = 52$ μs. In this case, an exponential filter with decay time 250 ms is applied.

sources are dedicated to transmitter (2.5 V), receiver (1.5 V), tuning and matching in variable frequency probes (± 25 V). A multifunction board (NI PCe-6259) is used for generation of TX/RX TTL switching pulse and signal acquisition. All experimental parameters T_R and τ (V_m and V_t for external coil) are controlled by a LabVIEW program.

IV. RESULTS

A. Noise and gain

The gain of the receiver, measured by looking at the amplification of a controlled input voltage signal, is 54 dB in agreement with simulations within 2 dB in the frequency range 1-300 MHz. The simulated input referred noise of the receiver is $n_{elec} \approx 1.1$ nV/Hz$^{1/2}$ within its bandwidth. When an external coil is matched to 320 Ω, the equivalent impedance at LNA input is 160 Ω, resulting from the parallel between 320 Ω and R_m. In these conditions, the overall receiver input noise is expected to be 2 nV/Hz$^{1/2}$. When we consider the 60 Ω integrated coil, the input noise is given by n_{elec} and the coil itself. The expected input noise in this condition is 1.5 nV/Hz$^{1/2}$. Fig. 4 is a measurement of the input noise voltage spectral density (VSD) for both cases, showing good agreement with the expected values.

The effective noise figure can be defined as the factor by which the SNR originally given by the coil is degraded. When an external coil is matched to the real input impedance of the receiver, the SNR is degraded by 3 dB, a factor paid to opportunely protect the LNA using 320 Ω at input. A further degradation of 2 dB is added by the electronic noise of the receiver. This relatively large factor is due to the trade-off between the wide bandwidth operation (1-300 MHz) and the low input referred noise, as explained in detail in the supplementary material.[27] The total effective noise figure with external coil is thus 5 dB. In the fully integrated probe, the electronic noise is approximately equal to the thermal noise of the microcoil, giving an effective noise figure of 3 dB.

B. Multi-nuclear NMR spectroscopy

In this section, we show the application of our single-chip transceiver to multi-nuclear NMR mass-limited spectroscopy. Our multi-nuclear probe with external coil is a multi-frequency probe as shown in Fig. 2(a), where the coil is a 14 turns solenoid made by an enameled copper wire ($\phi = 100$ μm) wrapped around a fused silica capillary having an external diameter of 450 μm and internal one of 320 μm. Its inductance is $L = 60$ nH and its unitary field is $B_u = 0.012$ T/A at 300 MHz.
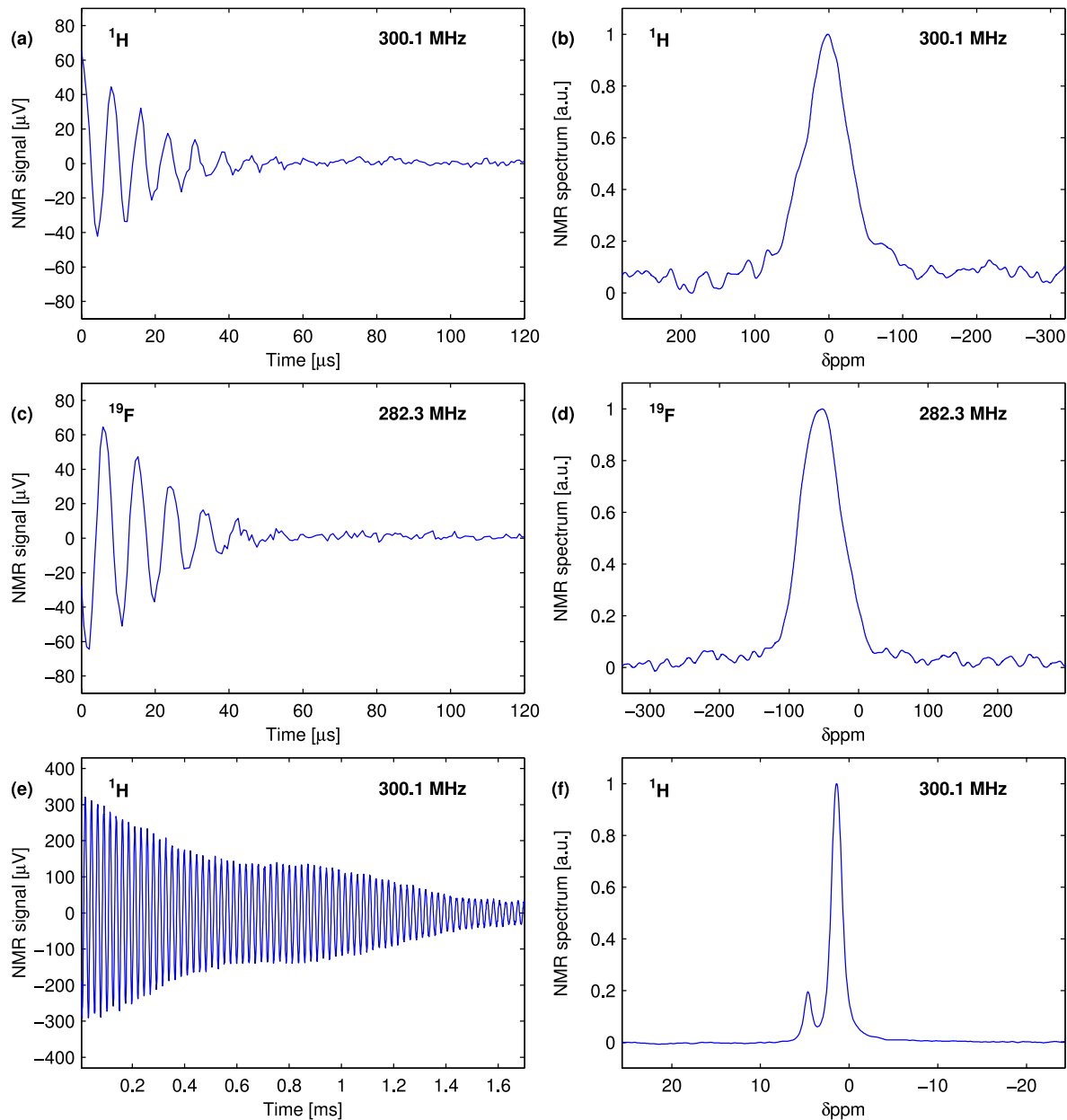
FIG. 6. Measurements with the integrated coil in a field $B_0 = 7.05$ T. (a) Time domain signal of ^{1}H at chip output, average of 5000 measurements with $T_R = 14$ s and $\tau = 2$ μs. (b) ^{1}H spectrum. (c) Time domain signal of ^{19}F at chip output, average of 5000 measurements with $T_R = 8$ s and $\tau = 2$ μs. (d) ^{19}F spectrum. Spectra are FFT real parts obtained from a solid sample of H$_4$F$_6$NP placed on the micro-coil shown in Fig. 1(a). The sample is a grain of about 130 pl. An exponential filter with decay time 100 μs is applied. (e) Time domain signal of ^{1}H at chip output, average of 3000 measurements with $T_R = 1$ s and $\tau = 2$ μs. (f) ^{1}H spectrum. The sample is about 250 pl of solid *cis*-polyisoprene. An exponential filter with decay time 2 ms is applied. (a)-(f) The AF external gain is 10^3 and the antialiasing filter frequency is 300 kHz. The acquisition is performed with sampling rate of 1 MHz. 9 μs of data are rejected. Each signal is down-converted within 50 and 150 kHz.

The resonator resistance is dominated by the resistance of the diodes and their connection to the coil, and it is estimated at about 2 Ω at 300 MHz. During the fabrication, no glue is used to fix the wire on the capillary. The coil is inserted into a 2 ml Eppendorf tube (BRAND® microcentrifuge tube, φ = 1 cm) later filled with D$_2$O for susceptibility matching.[26] In our case, the best achieved full width at half maximum of the ^{1}H spectrum goes from about 50 Hz to 6 Hz when the susceptibility matching fluid is added.

In Fig. 5, we show the real part of the spectra taken from a sample of 7.5 M of NaBF$_4$ dissolved in H$_2$O. NMR experiments on this system have been reported previously.[32] J-splitting of

^{19}F and ^{11}B has 1:1:1:1 primary peaks for fluorine and 1:4:6:4:1 for boron with relative shifts of about 5 Hz at 7 M concentration. These peaks arise from the J-coupling between ^{19}F (I = 1/2) and ^{11}B (I = 3/2) spins in the BF$_4^-$ molecule. Fig. 5(a) shows the ^{1}H spectrum due to H$_2$O. Fig. 5(b) shows the ^{19}F spectrum, where the four peaks due to ^{11}B are visible, while a second unresolved structure arises from the presence of ^{10}B isotope (I = 3). Fig. 5(c) shows the ^{11}B spectrum, with the five peaks due to the possible configurations of four equivalent ^{19}F spins. Finally, the single peak in Fig. 5(d) arises from Na$^+$ ions. All chemical shifts are expressed in ppm deviation from the resonance frequency of standard reference samples, using for

each nucleus the values reported in Ref. 33. Since these reference molecules were not present in our sample, we assigned a chemical shift of 4.79 ppm to the ^{1}H peak of H_2O, thus computing the resonance frequency of the ^{1}H reference sample. This allows to determine the chemical shifts for all nuclei with respect to their usual references as suggested in Ref. 33.

Fig. 6 shows measurements performed with the integrated microcoil of Fig. 1(a). No stabilization system acts on the magnetic field, whose typical drift during twenty hours is below 60 nT (9 ppb). In Figs. 6(a)-6(d), the sample is a grain of ammonium hexafluorophosphate (216593, Sigma Aldrich). Both ^{19}F and ^{1}H signals show a relaxation time of about 30 μs. These measurements on a solid sample were possible thanks to the short dead-time of our probe. Figs. 6(e) and 6(f) show measurements on a sample of *cis*-polyisoprene (182141, Sigma Aldrich). Due to a relatively important chain segmental mobility, *cis*-polyisoprene has a ^{1}H-NMR resonance line significantly narrower with respect most of solid samples. Fig. 6(f) shows the real part of the FFT, to which the three groups CH, CH_2, and CH_3 contribute. The main peak is given by groups CH_2 and CH_3, the secondary one by CH.[34] All chemical shifts are expressed in ppm deviation from the resonance frequency of standard reference samples, using for each nucleus the values reported in Ref. 33. Since these reference molecules were not present in our sample, we assigned a chemical shift of 1.5 ppm to the ^{1}H peak of CH_2 and CH_3 and assumed the same field B_0 for both samples.

In a pulse of length τ, there are frequencies up to an offset from carrier of about $1/\tau$ and, in multi-nuclear experiments on unknown samples, the employed pulse lengths should be short enough to excite resonance at all the possible chemical shifts. Thus, the ability of transmitting power to the coil can be critical for the excitation of broad spectra. In Table I, we report the measured $\tau_{\pi/2}$. For the external coil, the measured pulse lengths are in agreement with SPICE simulations of the transmission condition using, for varactor diodes, the models provided by manufacturers. By comparison with simulations performed with fixed capacitors, we concluded that the use of varactor diodes increases the $\tau_{\pi/2}$ length by a factor of 1.3.

Using an external coil, it is possible to cover the whole chemical shift ranges in experiments performed on ^{1}H, ^{11}B, ^{23}Na at $\vartheta = \pi/2$, being their chemical shifts 20 kHz at most at 7 T. For ^{19}F, $\tau_{\pi/2} = 14$ μs is slightly too long for this critical aim, being its chemical shifts over a range of 280 kHz at 7 T. Possible solutions to this issue are to increase the transmitted power designing the transmitter with RF integrated circuit technologies which operate at higher voltages or to increase the unitary field of the coil using a thinner wire or a different design.

With the integrated coil shown in Fig. 1(a), the obtained $\tau_{\pi/2} = 2$ μs is short enough for the uniform excitation of broad chemical shifts such that of the ^{19}F nucleus.

In Table I, we report the theoretical and experimental values of the signal amplitudes s_0 and noise VSD at chip output. Based on s_0 and VSD, it is possible to express the sensitivity of the probe in terms of nuclear spins. The spin sensitivity N_{min}, defined as $N_{min} = V_s N_s VSD/s_0$, is equal to the number of nuclear spins which give a time-domain SNR of 1 considering a noise equivalent bandwidth of 1 Hz. This quantity expresses

TABLE I. Performances and characteristics of the multi-nuclear probes. υ_0: resonance frequency, $\tau_{\pi/2}$: $\pi/2$ nutation pulse length (see equation in Sec. II D), N_{min}: spin sensitivity (see equation in Sec. IV B), s_0: signal amplitude at chip output, VSD: noise voltage spectral density at chip output. Theoretical values are in parenthesis.

	υ_0 (MHz)	$\tau_{\pi/2}$ (μs)	s_0 (mV)	VSD (μV/Hz$^{1/2}$)	N_{min} (Hz$^{-1/2}$)
External coil (7.5 M NaBF$_4$ in H$_2$O)					
^{1}H	300.1	12	35	0.6	10^{14}
		(9)	(50)	(0.5)	(8×10^{13})
^{19}F	282.3	14	15.5	0.6	10^{14}
		(10)	(17.5)	(0.5)	(8×10^{13})
^{11}B	96.3	32	6	0.9	8×10^{14}
		(29)	(10)	(0.7)	(4×10^{14})
^{23}Na	79.4	52	5	0.9	10^{15}
		(35)	(8)	(0.7)	(6×10^{14})
Integrated coil (H$_4$F$_6$NP)					
^{1}H	300.1	2	0.11	0.32	1.5×10^{13}
		(2)	(0.1)	(0.35)	(1.5×10^{13})
^{19}F	282.3	2	0.13	0.32	1.5×10^{13}
		(2)	(0.14)	(0.35)	(1.5×10^{13})
Integrated coil (*cis*-polyisoprene)					
^{1}H	300.1	2	0.34	0.32	1.5×10^{13}
		(2)	(0.36)	(0.35)	(1.5×10^{13})

unambiguously the capability of the probe to sense nuclear spins, independently from the effective relaxation time T_2^* and the number of spectral lines. From the value N_{min}, it is possible to compute the expected SNR in the frequency domain, once the distribution of the spectral lines of the sample and the effective relaxation time are known. We note that the sensitivity of the fully integrated probe surpasses by an order of magnitude the one of the external coil, proving the advantage of having a larger B_u. For the fully integrated probe, the unitary field in proximity to the center of the coil is $B_u = 250$ mT/A. For the external solenoid, $B_u = 12$ mT/A. As shown in Table I, our integrated probe achieves a ^{1}H spin sensitivity N_{min} of about 1.5×10^{13} spins/Hz$^{1/2}$ at 300 MHz, which represents probably the best spin sensitivity reported to date.

Since the gain and input VSD scale by approximately the same factor up to 1 GHz, we expect a ^{1}H spin sensitivity of 2×10^{12} spins/Hz$^{1/2}$ at 1 GHz.

V. DISCUSSION

In this work, we proposed a 1 mm^2 broadband single-chip transceiver for multi-frequency pulsed NMR probes. On a scale of sample volumes of 100 nl, we used reversed biased diodes as tuning and matching elements to realize multi-frequency LC resonators. On a scale of sample volumes smaller than 500 pl, we used a non-resonant integrated microcoil. As a result, we obtained simple, but effective and versatile, low-cost electronic interfaces for NMR probes with high spin sensitivities.

The fully integrated TX/RX switch allows minimization of off-chip discrete components, while the broadband nature

of the transceiver allows its use in multi-nuclear probes as the ones described above. We demonstrated the versatility of this approach by showing its use for multi-nuclear NMR spectroscopy on both liquid and solid samples.

Given that the use of short pulse lengths is a key feature needed by pulsed NMR probes, we discussed the problem of having a fixed limited power during transmission. We concluded that experiments in mass-limited conditions can be applied at their best in both resonant and non-resonant probes thanks to the high field per unit current produced by microcoils.

Apart from size reduction, the use of integrated CMOS transceivers for NMR pulsed probes might have many practical advantages to manufacturers, such as to avoid the search of non-magnetic electronic components and possibly reduce costs. As future prospective, our work can serve as base to realize simple low-cost NMR interfaces and high sensitivity micro-probes arrays for micro-imaging and mass limited spectroscopy purposes.

[1]P. T. Callaghan, *Principles of Nuclear Magnetic Resonance Microscopy* (Clarendon Press, Oxford, 1991).

[2]A. Abragam, *The Principles of Nuclear Magnetic Resonance* (Clarendon Press, Oxford, 1961).

[3]I. L. Pykett, Sci. Am. **246**(5), 78 (1982).

[4]R. Haken and B. Blumich, J. Magn. Reson. **144**(2), 195 (2000).

[5]H. Lee, E. Sun, D. Ham, and R. Weissleder, Nat. Med. **14**(8), 869 (2008).

[6]K. M. Lei, P. I. Mak, M. K. Law, and R. P. Martins, Analyst **139**(23), 6204 (2014).

[7]H. Kuhn, M. Klein, A. Wiesmath, D. E. Demco, B. Blumich, J. Kelm, and P. W. Gold, Magn. Reson. Imaging **19**(3-4), 497 (2001).

[8]R. Sacchi, F. Addeo, and L. Paolillo, Magn. Reson. Chem. **35**, S133 (1997).

[9]See http://picospin.com/ for bench-top NMR spectrometers.

[10]See http://www.nmr-mouse.de/ for NMR-MOUSE systems.

[11]P. J. Mohr, B. N. Taylor, and D. B. Newell, J. Phys. Chem. Ref. Data **41**(4), 043109 (2012).

[12]D. I. Hoult and R. E. Richards, J. Magn. Reson. **24**(1), 71 (1976).

[13]H. S. Gutowsky, L. H. Meyer, and R. E. McClure, Rev. Sci. Instrum. **24**(8), 644 (1953).

[14]K. Halbach, Nucl. Instrum. Methods **169**(1), 1 (1980).

[15]E. Danieli, J. Perlo, B. Blumich, and F. Casanova, Angew. Chem., Int. Ed. **49**(24), 4133 (2010).

[16]N. Sun, T. J. Yoon, H. Lee, W. Andress, R. Weissleder, and D. Ham, IEEE J. Solid-State Circuits **46**(1), 342 (2011).

[17]D. Ha, J. Paulsen, N. Sun, Y.-Q. Song, and D. Ham, Proceedings of the National Academy of Sciences **111**, 11955 (2014).

[18]J. Kim, B. Hammer, and R. Harjani, *2012 IEEE Custom Integrated Circuits Conference (CICC)* 2012.

[19]N. Sun, Y. Liu, H. Lee, R. Weissleder, and D. Ham, IEEE J. Solid-State Circuits **44**(5), 1629 (2009).

[20]J. Anders, G. Chiaramonte, P. SanGiorgio, and G. Boero, J. Magn. Reson. **201**(2), 239 (2009).

[21]T. Cherifi, N. Abouchi, G. N. Lu, L. Bouchet-Fakri, L. Quiquerez, B. Sorli, J. F. Chateaux, M. Pitaval, and P. Morin, IEEE Trans. Circuits Syst. I: Regular Pap. **52**(12), 2576 (2005).

[22]J. Anders, P. SanGiorgio, X. Deligianni, F. Santini, K. Scheffler, and G. Boero, Magn. Reson. Med. **67**(1), 290 (2012).

[23]J. Anders, P. SanGiorgio, and G. Boero, J. Magn. Reson. **209**(1), 1 (2011).

[24]G. Boero, J. Frounchi, B. Furrer, P. A. Besse, and R. S. Popovic, Rev. Sci. Instrum. **72**(6), 2764 (2001).

[25]R. M. Fratila, M. V. Gomez, S. Sykora, and A. H. Velders, Nat. Commun. **5**, 3025 (2014).

[26]D. L. Olson, T. L. Peck, A. G. Webb, R. L. Magin, and J. V. Sweedler, Science **270**(5244), 1967 (1995).

[27]See supplementary material at http://dx.doi.org/10.1063/1.4916206 for details on electronics.

[28]T. H. Lee, *The Design of CMOS Radio-Frequency Integrated Circuits* (Cambridge university press, 2004).

[29]W. G. Proctor and F. C. Yu, Phys. Rev. **77**(5), 717 (1950).

[30]E. L. Hahn, Phys. Rev. **80**(4), 580 (1950).

[31]N. Bloembergen, E. M. Purcell, and R. V. Pound, Phys. Rev. **73**(7), 679 (1948).

[32]K. Kuhlmann and D. M. Grant, J. Phys. Chem. **68**(11), 3208 (1964).

[33]R. K. Harris, E. D. Becker, S. M. C. Menezes, P. Granger, R. E. Hoffman, and K. W. Zilm, Pure Appl. Chem. **80**(1), 59 (2008).

[34]H. Sato and Y. Tanaka, J. Polym. Sci., Part A: Polym. Chem. **17**(11), 3551 (1979).